IEEE Access
Multidisciplinary | Rapid Review | Open Access Journal

Received May 24, 2022, accepted June 16, 2022, date of publication June 21, 2022, date of current version June 24, 2022.

Digital Object Identifier 10.1109/ACCESS.2022.3184706

Performance Assessment of Millimeter-Wave NOMA System With Intelligent Reflecting Surface

NGUYEN VAN VINH[1] **AND PHAN VAN TRI**[2]
[1]Department of Information Assurance (IA), FPT University, Hanoi 100000, Vietnam
[2]Academy of Cryptography Techniques, Hanoi 100000, Vietnam

Corresponding author: Phan Van Tri (phanvantri@actvn.edu.vn)

ABSTRACT This paper analyzes the performance of millimeter-wave (mmWave) non-orthogonal multiple access (NOMA) system with the aid of an intelligent reflecting surface (IRS). We derive the outage probability (OP) expressions at two users D_1 and D_2 of the IRS aided mmWave-NOMA system (the IRS-mmWave-NOMA system in the following). We validate the derived expressions via computer simulations. By considering the Nakagami-m fading channels and the path loss model proposed for 5G standard in the IRS-mmWave-NOMA system, our results are more suitable in practical scenarios. Specifically, numerical results observe that even the carrier frequency is extremely high ($f_c = 90$ GHz) and the transmitter-receiver distances are further than 50 m, the OPs at D_1 and D_2 can achieve 10^{-4} when the transmit power of base station (BS) is 30 dBm (dB in the following). Moreover, the OPs at D_1 and D_2 with IRS are greatly lower than OPs without IRS. This result demonstrates the huge benefits of utilizing IRS in mmWave-NOMA system. In addition, we can use an IRS with larger number of reflecting elements to maintain the OP performance at D_1 and D_2 when the distances are increased and f_c is higher. On the other hand, we should choose a suitable value of power allocation coefficients to obtain the same performance at D_1 and D_2.

INDEX TERMS Non-orthogonal multiple access, millimeter-wave, intelligent reflecting surface, moment function, outage probability.

I. INTRODUCTION

Under the fast developments of wireless networks, especially in the beyond 5G (B5G) of mobile communications, the available frequency bands may not satisfy the high capacity demand in practice. In this circumstance, millimeter-wave (mmWave) communications become a key technology [1], [2]. It is because mmWave communication systems use frequency from 30 GHz to 300 GHz. Thus, they can support ultra-high transmission rate and massive connectivity [3], [4]. Consequently, the propagation characteristics as well as the applied scenarios of the mmWave communications have been intensively determined [5], [6].

Besides mmWave communications, non-orthogonal multiple access (NOMA) is a new technology that enables to aid multi-user in the same code, frequency, and time resources [7]. Specifically, the transmitter uses superposition coding in the power domain for transmitting multi-message to multi-user. At the user, successive interference cancellation (SIC) is used to distinguish and subtract messages of other users [3]. As the results, the capacity and the number of users of NOMA systems are significantly higher than those of classical orthogonal multiple access (OMA) systems [8], [9]. Therefore, applying NOMA scheme in B5G systems has attracted attention in both industry and academy [7], [9], [10].

Recently, mmWave communications and NOMA technology are combined in wireless systems. [3]–[6], [11]–[13]. Specifically, the energy efficiency, outage probability (OP), and sum rate were derived in mmWave-NOMA system with multiple base stations [4]. Compared with traditional NOMA systems, mmWave-NOMA communications lead to a significant increase in computational complexity. It is because the OP expression of mmWave-NOMA communications is very complex [4]. Moreover, the performance of mmWave-NOMA and mmWave-OMA systems were compared [13]. It was demonstrated that mmWave-NOMA not only outperforms mmWave-OMA but also has good flexibility.

On the other hand, intelligent reflecting surface (IRS) has recently become a key solution in B5G networks due to its advantages. Specifically, IRS significantly enhances the performance of wireless systems without power supply,

The associate editor coordinating the review of this manuscript and approving it for publication was Amjad Mehmood.

signal processing, and converters [14]–[19]. Moreover, the IRS can work at any frequency. Thus, it can help to significantly reduce the effects of unfavorable parameters induced by high frequencies and far distances between transmitter and receiver in the mmWave communications [6], [14], [20]. In particular, the OP with IRS is greatly lower than OP with classical relay when they are deployed in wireless systems [16], [21]. Additionally, the energy efficiency is significantly improved by utilizing IRS instead of relay. Furthermore, the performance of the IRS aided wireless systems over Nakagami-*m* fading channels was also studied such as in [22] and [23]. However, the works in [22] and [23] considered only one user and without mmWave communications. Thus, the advantages of NOMA technology and mmWave communications were not exploited. Due to the huge benefits of the IRS, it is recently combined with NOMA technology for dramatically improving the capacity and quality of service of wireless systems [20], [24]–[37]. However, the specific carrier frequencies used for system operations were ignored in these reports. Nowadays, the IRS is combined with mmWave-NOMA communications for greatly improving the system performance [6]. Particularly, power allocation problem and hybrid beamforming were formulated for maximizing the sum rate of the system. However, the mathematical expressions such as OP were not obtained in [6] to gain useful insights in the system behaviors.

As the aforementioned, the mmWave, NOMA, and IRS technologies have many benefits and they can be combined and deployed in B5G of wireless systems. However, the research on the combining of mmWave, NOMA, and IRS is still lack of, especially in terms of mathematical analysis. Specifically, the mmWave-NOMA communications suffer the path loss and signal blockage [6]. In this circumstance, utilizing IRS can solve these issues. On the other hand, the effects of system parameters such as frequency and distances on the performance of IRS aided mmWave-NOMA systems were not well studied. In particular, most of previous works normalized the channel gains between base station and NOMA users [32], [35], [37], [38]. In other words, the effects of carrier frequency, distances, and antenna gains were neglected when analyzing the performance of the IRS aided NOMA systems. Thus, their results were not suitable in practical scenarios due to the great impacts of those parameters. Importantly, the 5G and B5G networks use mmWave communications. Therefore, it is important to use the channel model proposed for 5G and B5G standard. These problems motivate us to investigate an IRS aided mmWave-NOMA system (the IRS-mmWave-NOMA system in the following). In particular, besides exploiting IRS for aiding NOMA users, the direct base station-user links are also exploited in the IRS-mmWave-NOMA system. So far, this is the first work exploiting mmWave communications in the IRS aided NOMA system in terms of mathematical analysis. Therefore, our results can be applied for mmWave-NOMA systems with IRS and without direct links, without IRS and with direct links. The main contributions of this paper can be summarized as follows:

- We determine an IRS-mmWave-NOMA system where base station (BS) transmits signal to two NOMA users using frequency of mmWave communications. Both far and near users combine signals via direct and reflected paths for enhancement of received signal power. We consider the channel model proposed for 5G standard, thus, the considered IRS-mmWave-NOMA system is more suitable in practice.
- We derive the expressions of OP at two users D_1 and D_2 of the IRS-mmWave-NOMA system over Nakagami-*m* fading channels. We observe that the combination of direct and reflected paths leads to a significant increase in mathematical computations. However, by exploiting them, the performance at D_1 and D_2 is considerably improved. We validate the derived expressions via Monte-Carlo simulations by using PC running MATLAB.
- We investigate the OP at D_1 and D_2 in practical scenarios. Numerical results clarify that the usage of IRS considerably enhances the OP performance at D_1 and D_2. Specifically, the effects of scientific parameters such as the carrier frequency, distances, and antenna gains on the OP at D_1 and D_2 in the IRS-mmWave-NOMA system are deeply determined. In particular, the OPs at D_1 and D_2 with IRS can achieve 10^{-4} when the transmit power of BS is 30 dBm even the carrier frequency is extremely high ($f_c = 90$ GHz) and the BS-user distances is further than 50 m. Moreover, increasing distances or f_c significantly reduces the performance at both users due to the properties of mmWave communications. Additionally, depending on the number of reflecting elements on the IRS and the distances between BS-users, we can choose a specific value of power allocation coefficient of NOMA scheme to obtain the same performance at D_1 and D_2.

The rest of this paper is organized as follows. Section II presents the system and signal models, where D_1 and D_2 receive signals transmitted from BS via direct paths and reflect paths from IRS. Section III focuses on mathematical analysis, where OP expressions at D_1 and D_2 are detailedly derived. Section IV provides numerical results to obtain the behaviors of IRS-mmWave-NOMA system. Finally, Section V concludes our works.

II. SYSTEM MODEL

Fig. 1 depicts the block diagram of the IRS-mmWave-NOMA system, where base station (BS) transmits signals to two NOMA users (D_1 and D_2) using bandwidth of mmWave. An IRS (I) is used to support the communications from S to D_1 and D_2. D_1/D_2 receive signals transmitted from BS via both direct BS-D_1/BS-D_2 channels and reflected BS-I-D_1/BS-I-D_2 channels. D_1 is the far user while D_2 is the near user. All transceivers are quipped with single antenna

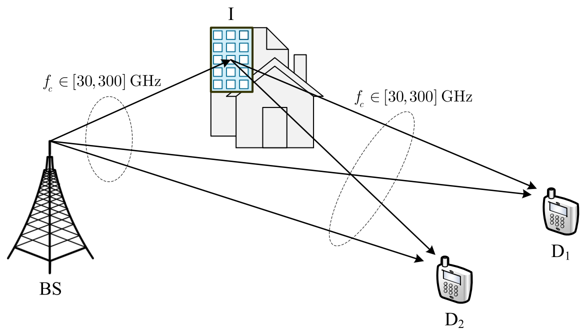

FIGURE 1. Block diagram of the IRS-mmWave-NOMA system.

while I is equipped with L reflecting elements. In practice, a controller is often used in the IRS to adjust its phases [39].

Thanks to the NOMA principles, BS transmits signal combining two separate messages for users D_1 and D_2 based on the power domain, e.g., $x_{BS} = \sqrt{a_1 P_{BS}} x_1 + \sqrt{a_2 P_{BS}} x_2$, where a_1 and a_2 are, respectively, the power allocation coefficients of D_1 and D_2 with $a_1 > a_2$ and $a_1 + a_2 = 1$; P_{BS} denotes the average transmit power of BS.

The received signal at user D_i ($i \in \{1, 2\}$) is expressed as

$$y_{D_i} = \left(\sum_{l=1}^{L} h_l g_{li} e^{j\varphi_l} + h_{BSD_i}\right) \sum_{k=1}^{2} \sqrt{a_k P_{BS}} x_k + z_{D_i}, \quad (1)$$

where h_l, g_{li}, and h_{BSD_i} are, respectively, the BS-I, I-D_i, and BS-D_i channels; φ_l is the phase of the lth reflecting element; $z_{D_i} \sim \mathcal{CN}(0, \sigma_i^2)$ is the Gaussian noise at D_i.

Using magnitudes and phases of complex numbers, we have $h_l = |h_l| e^{-j\theta_l}$, $g_{li} = |g_{li}| e^{-j\psi_{li}}$, $h_{BSD_i} = |h_{BSD_i}| e^{-j\phi_{BSD_i}}$, where $|h_l|$, $|g_{li}|$, and $|h_{BSD_i}|$ are, respectively, the magnitudes of h_l, g_{li}, and h_{BSD_i}; θ_l, ϕ_{BSD_i}, and ψ_{li} are, respectively, the phases of h_l, g_{li}, and h_{BSD_i}. Then, the received signal at user D_i is rewritten as

$$\begin{aligned} y_{D_i} &= \left(\sum_{l=1}^{L} |h_l||g_{li}| e^{j\varphi_l - j\theta_l - j\psi_{li}} + |h_{BSD_i}| e^{-\phi_{BSD_i}}\right) \\ &\quad \times \sum_{k=1}^{2} \sqrt{a_k P_{BS}} x_k + z_{D_i} \\ &= e^{-\phi_{BSD_i}} \left(\sum_{l=1}^{L} |h_l||g_{li}| e^{j(\varphi_l + \phi_{BSD_i} - \theta_l - \psi_{li})} + |h_{BSD_i}|\right) \\ &\quad \times \sum_{k=1}^{2} \sqrt{a_k P_{BS}} x_k + z_{D_i}. \end{aligned} \quad (2)$$

Let $\vartheta_{li} = \varphi_l + \phi_{BSD_i} - \theta_l - \psi_{li}$, (2) becomes

$$\begin{aligned} y_{D_i} &= e^{-\phi_{BSD_i}} \left(\sum_{l=1}^{L} |h_l||g_{li}| e^{j\vartheta_{li}} + |h_{BSD_i}|\right) \\ &\quad \times \sum_{k=1}^{2} \sqrt{a_k P_{BS}} x_k + z_{D_i}. \end{aligned} \quad (3)$$

Since the IRS is controlled by a controller that can adjust the IRS phases for maximizing the received signal power [16], [39]–[41]. Specifically, the phase of the IRS (φ_l) is picked up from a discrete phase set to obtain $\vartheta_{li} = 0$ [40], [41]. As a result, we have $\varphi_l + \phi_{BSD_i} - \theta_l - \psi_{li} = 0$. In other words, the phase of the IRS is expressed as

$$\varphi_l = -\phi_{BSD_i} + \theta_l + \psi_{li}. \quad (4)$$

It is worth noticing that (4) is widely applied not only an IRS but also multi-IRS aided wireless networks [16], [38]–[41]. On the other hand, (4) is taken for the ith user, thus, its received signal power can be maximized. However, the received signal power at the kth user ($i, k \in \{1, 2\}$ and $i \neq k$) may not be maximized [27]. In other words, the IRS is configured to maximize the received signal power at either D_1 or D_2 in the IRS-mmWave-NOMA system.

Using (4), (3) now is

$$\begin{aligned} y_{D_i} &= e^{-\phi_{BSD_i}} \left(\sum_{l=1}^{L} |h_l||g_{li}| + |h_{BSD_i}|\right) \\ &\quad \times \sum_{k=1}^{2} \sqrt{a_k P_{BS}} x_k + z_{D_i}. \end{aligned} \quad (5)$$

Based on NOMA principle, the far user D_1 detects its message by considering the near user's message as interference. Meanwhile, the near user D_2 has to detect D_1's message firstly. Then, it subtracts x_1 using SIC [38]. After that, it detects its message x_2. Consequently, the SINRs at D_1 for detect x_1 (denoted by ρ_{D_1}), D_2 for SIC x_1 (denoted by $\rho_{D_2}^{x_1}$) and detect x_2 (denoted by $\rho_{D_2}^{x_2}$) are, respectively, computed as

$$\rho_{D_1} = \frac{\left(\sum_{l=1}^{L} |h_l||g_{l1}| + |h_{BSD_1}|\right)^2 a_1 P_{BS}}{\left(\sum_{l=1}^{L} |h_l||g_{l1}| + |h_{BSD_1}|\right)^2 a_2 P_{BS} + \sigma^2}, \quad (6)$$

$$\rho_{D_2}^{x_1} = \frac{\left(\sum_{l=1}^{L} |h_l||g_{l2}| + |h_{BSD_2}|\right)^2 a_1 P_{BS}}{\left(\sum_{l=1}^{L} |h_l||g_{l2}| + |h_{BSD_2}|\right)^2 a_2 P_{BS} + \sigma^2}, \quad (7)$$

$$\rho_{D_2}^{x_2} = \frac{\left(\sum_{l=1}^{L} |h_l||g_{l2}| + |h_{BSD_2}|\right)^2 a_2 P_{BS}}{\sigma^2}. \quad (8)$$

It would be better to note that (6), (7), and (8) can be considered as the maximal SINRs at D_1 and D_2. It is because the IRS can adjust its phase to maximize the SINR at either D_1 or D_2. In particular, when the IRS is configured for D_1, the SINR at D_1 is given in (6) while the SINRs at D_2 may be lower than those given in (7) and (8). Similarly, when the IRS is configured for D_2, the SINRs at D_2 are given in (7) and (8) while the SINR at D_1 may be lower than that given in (6). However, in order to achieve the fairness of both NOMA users, we use the maximal SINRs at these two users for our analysis. This assumption was widely used in the literature such as in [27], [38], and [42]. Hence, the OP calculated from the maximal SINRs can be considered as the lower bound of the IRS aided NOMA systems.

In this paper, we use the Nakagami-m fading channels and mmWave bands in the IRS-mmWave-NOMA system, the CDF, PDF, and spread parameter of channel magnitude Δ, where $\Delta \in \{|h_l|, |g_{li}|, |h_{\mathrm{BSD}_i}|\}$ are, respectively, given as [40], [43]

$$F_\Delta(x) = \frac{1}{\Gamma(m_\Delta)}\gamma\Big(m_\Delta, \frac{m_\Delta}{\Omega_\Delta}x^2\Big) = 1 - \frac{1}{\Gamma(m_\Delta)}\Gamma\Big(m_\Delta, \frac{m_\Delta}{\Omega_\Delta}x^2\Big),\ x \geq 0, \tag{9}$$

$$f_\Delta(x) = \frac{2m_\Delta^{m_\Delta}}{\Gamma(m_\Delta)\Omega_\Delta^{m_\Delta}}x^{2m_\Delta-1}\exp\Big(-\frac{m_\Delta}{\Omega_\Delta}x^2\Big),\ x \geq 0, \tag{10}$$

$$\Omega_\Delta = -32.4 - 31.7\log(d_\Delta) - 20\log(f_c) + G_{\mathrm{tx}} + G_{\mathrm{rx}}, \tag{11}$$

where m_Δ and Ω_Δ are, respectively, the shape and spread parameters; d_Δ is the distance between the transmitter and receiver; $fc \geq 30$ GHz is the carrier frequency; $G_{\mathrm{tx}}/G_{\mathrm{rx}}$ are the transmitter/receiver antenna gains.[1]

III. PERFORMANCE ANALYSIS

In this section, we firstly calculate the mathematical expressions of the OPs at two NOMA users. Then the asymptotic expressions are derived to gain more insights in the behaviors of the IRS-mmWave-NOMA system.

A. OUTAGE PROBABILITY ANALYSIS

The OPs at D_1 and D_2 are, respectively, expressed as

$$\mathcal{P}_{\mathrm{D}_1} = \Pr\left\{\rho_{\mathrm{D}_1} < \gamma_{\mathrm{th}}\right\}, \tag{12}$$

$$\mathcal{P}_{\mathrm{D}_2} = \Pr\left\{\min\{\rho_{\mathrm{D}_2}^{x_1}, \rho_{\mathrm{D}_2}^{x_2}\} < \gamma_{\mathrm{th}}\right\}, \tag{13}$$

where ρ_{D_1}, $\rho_{\mathrm{D}_2}^{x_1}$, and $\rho_{\mathrm{D}_2}^{x_2}$ are, respectively, given in (6), (7), and (8); γ_{th} is the SINR threshold.

Replacing (6) into (12), (7) and (8) into (13), the OPs at D_1 and D_2 are, respectively, calculated as (14) and (15), as shown at the bottom of the next page. From these expressions, we obtain the OPs at D_1 and D_2 of the IRS-mmWave-NOMA system in the following Theorem.

Theorem: The OPs at D_1 and D_2 of the IRS-mmWave-NOMA system are, respectively, derived in (16) and (17), as shown at the bottom of the next page, where $\Theta_X(p)$ is the pth moment of X, e.g.,

$$\Theta_{\mathcal{H}_i}(1) = \Theta_{\mathcal{B}_i}(1) + \Theta_{|h_{\mathrm{BSD}_i}|}(1), \tag{18}$$

$$\Theta_{\mathcal{H}_i}(2) = \Theta_{\mathcal{B}_i}(2) + \Theta_{|h_{\mathrm{BSD}_i}|}(2) + 2\Theta_{\mathcal{B}_i}(1)\Theta_{|h_{\mathrm{BSD}_i}|}(1), \tag{19}$$

$\Theta_{|h_{\mathrm{BSD}_i}|}(1)$, $\Theta_{|h_{\mathrm{BSD}_i}|}(2)$, $\Theta_{\mathcal{B}_i}(1)$, and $\Theta_{\mathcal{B}_i}(2)$ ($i \in \{1,2\}$) are, respectively, given as (21), (22), (29), and (30).[2]

Proof: Based on the CDF and PDF given in (9) and (10), the pth moments of $|h_{\mathrm{BSD}_1}|$ and $|h_{\mathrm{BSD}_2}|$ are, respectively, presented as

$$\Theta_{|h_{\mathrm{BSD}_i}|}(p) \triangleq \mathbb{E}\{|h_{\mathrm{BSD}_i}|^p\} = \frac{\Gamma(m_{|h_{\mathrm{BSD}_i}|} + p/2)}{\Gamma(m_{|h_{\mathrm{BSD}_i}|})}\Big(\frac{m_{|h_{\mathrm{BSD}_i}|}}{\Omega_{|h_{\mathrm{BSD}_i}|}}\Big)^{-p/2}, \tag{20}$$

From (20), the pth moments ($p \in \{1,2\}$) of $|h_{\mathrm{BSD}_i}|$ are obtained as

$$\Theta_{|h_{\mathrm{BSD}_i}|}(1) = \frac{\Gamma(m_{|h_{\mathrm{BSD}_i}|} + 1/2)}{\Gamma(m_{|h_{\mathrm{BSD}_i}|})}\sqrt{\frac{\Omega_{|h_{\mathrm{BSD}_i}|}}{m_{|h_{\mathrm{BSD}_i}|}}}, \tag{21}$$

$$\Theta_{|h_{\mathrm{BSD}_i}|}(2) = \frac{\Gamma(m_{|h_{\mathrm{BSD}_i}|} + 1)}{\Gamma(m_{|h_{\mathrm{BSD}_i}|})}\frac{\Omega_{|h_{\mathrm{BSD}_i}|}}{m_{|h_{\mathrm{BSD}_i}|}} = \Omega_{|h_{\mathrm{BSD}_i}|}, \tag{22}$$

On the other hand, the PDF of $|h_l||g_{li}|$, $i \in \{1,2\}$ is computed as

$$f_{|h_l||g_{li}|}(y) = \int_0^\infty \frac{1}{z}f_{|g_{li}|}\Big(\frac{y}{z}\Big)f_{|h_l|}(z)\,dz. \tag{23}$$

Replacing the PDF given in (10) into (23), we have

$$f_{|h_l||g_{li}|}(y) = \frac{4}{\Gamma(m_{|h_l|})\Gamma(m_{|g_{li}|})}\Big(\frac{m_{|h_l|}}{\Omega_{|h_l|}}\Big)^{m_{|h_l|}}\Big(\frac{m_{|g_{li}|}}{\Omega_{|g_{li}|}}\Big)^{m_{|g_{li}|}} \times y^{2m_{|g_{li}|}-1}\int_0^\infty z^{2m_{|h_l|}-2\,m_{|g_{li}|}-1} \times \exp\Big(-\frac{m_{|h_l|}z^2}{\Omega_{|h_l|}} - \frac{y^2 m_{|g_{li}|}}{\Omega_{|g_{li}|}z^2}\Big)dz. \tag{24}$$

From [44, Eq. (3.478.4)], (24) is solved as

$$f_{|h_l||g_{li}|}(y) = \frac{4\Big(\frac{m_{|h_l|}m_{|g_{li}|}}{\Omega_{|h_l|}\Omega_{|g_{li}|}}\Big)^{\frac{m_{|h_l|}+m_{|g_{li}|}}{2}}}{\Gamma(m_{|h_l|})\Gamma(m_{|g_{li}|})}y^{m_{|h_l|}+m_{|g_{li}|}-1} \times \mathcal{K}_{m_{|h_l|}-m_{|g_{li}|}}\Big(2y\sqrt{\frac{m_{|h_l|}m_{|g_{li}|}}{\Omega_{|h_l|}\Omega_{|g_{li}|}}}\Big). \tag{25}$$

Now, we calculate the pth moment of $|h_l||g_{li}|$ as

$$\Theta_{|h_l||g_{li}|}(p) \triangleq \mathbb{E}\{(|h_l||g_{li}|)^p\} = \int_0^\infty y^p f_{|h_l||g_{li}|}(y)dy. \tag{26}$$

From [44, Eq. (6.561.16)], (26) becomes

$$\Theta_{|h_l||g_{li}|}(p) = \Big(\frac{m_{|h_l|}m_{|g_{li}|}}{\Omega_{|h_l|}\Omega_{|g_{li}|}}\Big)^{\frac{-p}{2}} \times \frac{\Gamma(m_{|h_l|}+p/2)\Gamma(m_{|g_{li}|}+p/2)}{\Gamma(m_{|h_l|})\Gamma(m_{|g_{li}|})}. \tag{27}$$

[1]It is worth noticing that Ω_Δ given in (11) clarifies the effects of the distances, carrier frequency, and antenna gains on the performance of the IRS-mmWave-NOMA system. In contrast to this work, previous works often normalized Ω_Δ by setting $\Omega_\Delta = 1$ in their analysis [32], [35], [37], [38]. Consequently, their results have not fully characterized the system behaviors of the 5G and B5G networks. Moreover, (11) clearly indicates that higher carrier frequency in mmWave communications leads to smaller spread parameter. Therefore, it is very important to investigate the mmWave communications in the IRS aided NOMA systems.

[2]Although the OP expressions at D_1 and D_2 given in (16) and (17) look like simple in overall, however, they include many complex terms. Therefore, the mathematical challenges in this paper are significant in comparison with previous works such as [37], [38].

Let $\mathcal{B}_i = \sum_{l=1}^{L} |h_l||g_{li}|$, the pth moment of $\mathcal{B}_i$ is expressed as

$$\begin{aligned}\Theta_{\mathcal{B}_i}(p) &\triangleq \mathbb{E}\{\mathcal{B}_i^p\}\\ &= \sum_{p_1=0}^{p}\sum_{p_2=0}^{p_1}\cdots\sum_{p_{L-1}=0}^{p_{L-2}}\binom{p}{p_1}\binom{p_1}{p_2}\cdots\binom{p_{L-2}}{p_{L-1}}\\ &\quad\times\Theta_{|h_l||g_{li}|}(p-p_1)\Theta_{|h_l||g_{li}|}(p_1-p_2)\cdots\Theta_{|h_l||g_{li}|}(p_{L-1}),\end{aligned} \tag{28}$$

where $\binom{a}{k} = \frac{a!}{k!(a-k)!}$.

From (27) and (28), the moments of $\mathcal{B}_i$ are computed as [45]

$$\Theta_{\mathcal{B}_i}(1) = \sum_{l=1}^{L}\Theta_{|h_l||g_{li}|}(1), \tag{29}$$

$$\Theta_{\mathcal{B}_i}(2) = \sum_{l=1}^{L}\Theta_{|h_l||g_{li}|}(2) + 2\sum_{l=1}^{L}\sum_{l'=l+1}^{L}[\Theta_{|h_l||g_{li}|}(1)]^2. \tag{30}$$

Let $\mathcal{H}_i = \mathcal{B}_i + |h_{\mathrm{BSD}_i}|$, its pth moment is

$$\begin{aligned}\Theta_{\mathcal{H}_i}(p) &\triangleq \mathbb{E}\{(\mathcal{B}_i + |h_{\mathrm{BSD}_i}|)^p\}\\ &= \mathbb{E}\left\{\sum_{p=0}^{t}\binom{t}{p}\mathcal{B}_i^p|h_{\mathrm{BSD}_i}|^{t-p}\right\}\\ &= \sum_{p=0}^{t}\binom{t}{p}\Theta_{\mathcal{B}_i}(p)\Theta_{|h_{\mathrm{BSD}_i}|}(t-p).\end{aligned} \tag{31}$$

From (31), the pth moments of $\mathcal{H}_i$ are given in (18) and (19).

Based on the pth moments of $\mathcal{H}_i$, we can derive the CDF of $\mathcal{H}_i$ as [40]

$$F_{\mathcal{H}_i}(x) \approx \frac{1}{\Gamma\left(\frac{[\Theta_{\mathcal{H}_i}(1)]^2}{\Theta_{\mathcal{H}_i}(2)-[\Theta_{\mathcal{H}_i}(1)]^2}\right)} \times\gamma\left(\frac{[\Theta_{\mathcal{H}_i}(1)]^2}{\Theta_{\mathcal{H}_i}(2)-[\Theta_{\mathcal{H}_i}(1)]^2}, \frac{\Theta_{\mathcal{H}_i}(1)x}{\Theta_{\mathcal{H}_i}(2)-[\Theta_{\mathcal{H}_i}(1)]^2}\right). \tag{32}$$

We should note that the approximation given in (32) has been widely used in the literature such as [37], [39], [40]. It was proved that the approximate and exact results perfectly match in low transmit power regime. However, there is a small difference between them in high transmit power regime.

Since $\Gamma(n, a) + \gamma(n, a) = \Gamma(n)$, (32) becomes

$$F_{\mathcal{H}_i}(x) \approx 1 - \frac{1}{\Gamma\left(\frac{[\Theta_{\mathcal{H}_i}(1)]^2}{\Theta_{\mathcal{H}_i}(2)-[\Theta_{\mathcal{H}_i}(1)]^2}\right)} \times\Gamma\left(\frac{[\Theta_{\mathcal{H}_i}(1)]^2}{\Theta_{\mathcal{H}_i}(2)-[\Theta_{\mathcal{H}_i}(1)]^2}, \frac{\Theta_{\mathcal{H}_i}(1)x}{\Theta_{\mathcal{H}_i}(2)-[\Theta_{\mathcal{H}_i}(1)]^2}\right). \tag{33}$$

Now, we reorganize (14) and (15) as

$$\mathcal{P}_{\mathrm{D}_1} = \Pr\left\{\mathcal{H}_1^2 P_{\mathrm{BS}}(a_1 - \gamma_{\mathrm{th}}a_2) < \gamma_{\mathrm{th}}\sigma^2\right\}. \tag{34}$$

$$\mathcal{P}_{\mathrm{D}_1} = \Pr\left\{\frac{\left(\sum_{l=1}^{L}|h_l||g_{l1}| + |h_{\mathrm{BSD}_1}|\right)^2 a_1 P_{\mathrm{BS}}}{\left(\sum_{l=1}^{L}|h_l||g_{l1}| + |h_{\mathrm{BSD}_1}|\right)^2 a_2 P_{\mathrm{BS}} + \sigma^2} < \gamma_{\mathrm{th}}\right\} = \Pr\left\{\left(\sum_{l=1}^{L}|h_l||g_{l1}| + |h_{\mathrm{BSD}_1}|\right)^2 P_{\mathrm{BS}}(a_1 - \gamma_{\mathrm{th}}a_2) < \gamma_{\mathrm{th}}\sigma^2\right\}. \tag{14}$$

$$\begin{aligned}\mathcal{P}_{\mathrm{D}_2} &= \Pr\left\{\min\left\{\frac{\left(\sum_{l=1}^{L}|h_l||g_{l2}| + |h_{\mathrm{BSD}_2}|\right)^2 a_1 P_{\mathrm{BS}}}{\left(\sum_{l=1}^{L}|h_l||g_{l2}| + |h_{\mathrm{BSD}_2}|\right)^2 a_2 P_{\mathrm{BS}} + \sigma^2}, \frac{\left(\sum_{l=1}^{L}|h_l||g_{l2}| + |h_{\mathrm{BSD}_2}|\right)^2 a_2 P_{\mathrm{BS}}}{\sigma^2}\right\} < \gamma_{\mathrm{th}}\right\}\\ &= \Pr\left\{\min\left\{\left(\sum_{l=1}^{L}|h_l||g_{l2}| + |h_{\mathrm{BSD}_2}|\right)^2 P_{\mathrm{BS}}(a_1 - \gamma_{\mathrm{th}}a_2), \left(\sum_{l=1}^{L}|h_l||g_{l2}| + |h_{\mathrm{BSD}_2}|\right)^2 a_2 P_{\mathrm{BS}}\right\} < \gamma_{\mathrm{th}}\sigma^2\right\}.\end{aligned} \tag{15}$$

$$\mathcal{P}_{\mathrm{D}_1} \approx \begin{cases} 1 - \frac{1}{\Gamma\left(\frac{[\Theta_{\mathcal{H}_1}(1)]^2}{\Theta_{\mathcal{H}_1}(2)-[\Theta_{\mathcal{H}_1}(1)]^2}\right)}\Gamma\left(\frac{[\Theta_{\mathcal{H}_1}(1)]^2}{\Theta_{\mathcal{H}_1}(2)-[\Theta_{\mathcal{H}_1}(1)]^2}, \frac{\Theta_{\mathcal{H}_1}(1)}{\Theta_{\mathcal{H}_1}(2)-[\Theta_{\mathcal{H}_1}(1)]^2}\sqrt{\frac{\gamma_{\mathrm{th}}\sigma^2}{P_{\mathrm{BS}}(a_1-\gamma_{\mathrm{th}}a_2)}}\right), & \gamma_{\mathrm{th}} < \frac{a_1}{a_2},\\ 1, & \gamma_{\mathrm{th}} \ge \frac{a_1}{a_2},\end{cases} \tag{16}$$

$$\mathcal{P}_{\mathrm{D}_2} \approx \begin{cases} 1 - \frac{1}{\Gamma\left(\frac{[\Theta_{\mathcal{H}_2}(1)]^2}{\Theta_{\mathcal{H}_2}(2)-[\Theta_{\mathcal{H}_2}(1)]^2}\right)}\Gamma\left(\frac{[\Theta_{\mathcal{H}_2}(1)]^2}{\Theta_{\mathcal{H}_2}(2)-[\Theta_{\mathcal{H}_2}(1)]^2}, \frac{\Theta_{\mathcal{H}_2}(1)}{\Theta_{\mathcal{H}_2}(2)-[\Theta_{\mathcal{H}_2}(1)]^2}\sqrt{\frac{\gamma_{\mathrm{th}}\sigma^2}{P_{\mathrm{BS}}a_2}}\right), & \gamma_{\mathrm{th}} \le \frac{a_1}{a_2} - 1,\\ 1 - \frac{1}{\Gamma\left(\frac{[\Theta_{\mathcal{H}_2}(1)]^2}{\Theta_{\mathcal{H}_2}(2)-[\Theta_{\mathcal{H}_2}(1)]^2}\right)}\Gamma\left(\frac{[\Theta_{\mathcal{H}_2}(1)]^2}{\Theta_{\mathcal{H}_2}(2)-[\Theta_{\mathcal{H}_2}(1)]^2}, \frac{\Theta_{\mathcal{H}_2}(1)}{\Theta_{\mathcal{H}_2}(2)-[\Theta_{\mathcal{H}_2}(1)]^2}\sqrt{\frac{\gamma_{\mathrm{th}}\sigma^2}{P_{\mathrm{BS}}(a_1-\gamma_{\mathrm{th}}a_2)}}\right), & \frac{a_1}{a_2} - 1 < \gamma_{\mathrm{th}} < \frac{a_1}{a_2},\\ 1, & \gamma_{\mathrm{th}} \ge \frac{a_1}{a_2},\end{cases} \tag{17}$$

$$\mathcal{P}_{D_2} = \Pr\left\{\min\left\{\mathcal{H}_2^2 P_{BS}(a_1-\gamma_{th}a_2), \mathcal{H}_2^2 a_2 P_{BS}\right\} < \gamma_{th}\sigma^2\right\}. \quad (35)$$

i) When $a_1-\gamma_{th}a_2 \le 0$ or $\gamma_{th} \ge a_1/a_2$, (34) and (35) are always true. It is because the left hand is ≤ 0 while the right hand is > 0. Consequently, $\mathcal{P}_{D_1} = \mathcal{P}_{D_2} = 1$ for $\gamma_{th} \ge a_1/a_2$.

ii) When $a_1-\gamma_{th}a_2 > 0$ or $\gamma_{th} < a_1/a_2$, we calculate $\mathcal{P}_{D_1}$ from (34) as

$$\begin{aligned}\mathcal{P}_{D_1} &= F_{\mathcal{H}_1^2}\left(\frac{\gamma_{th}\sigma^2}{P_{BS}(a_1-\gamma_{th}a_2)}\right)\\ &= F_{\mathcal{H}_1}\left(\sqrt{\frac{\gamma_{th}\sigma^2}{P_{BS}(a_1-\gamma_{th}a_2)}}\right).\end{aligned} \quad (36)$$

Based on (33), we derive the second line of (16) from (36). Combining of two cases, i.e., $\gamma_{th} < a_1/a_2$ and $\gamma_{th} \ge a_1/a_2$, we obtain (16).

Meanwhile, to obtain $\mathcal{P}_{D_2}$, we must investigate two sub-cases, e.g., $a_1-\gamma_{th}a_2 \ge a_2$ and $a_1-\gamma_{th}a_2 < a_2$.

If $a_1 - \gamma_{th}a_2 \ge a_2$ or $\gamma_{th} \le a_1/a_2 - 1$, we have $\min\{\mathcal{H}_2{}^2 P_{BS}(a_1-\gamma_{th}a_2), \mathcal{H}_2{}^2 a_2 P_{BS}\} = \mathcal{H}_2{}^2 a_2 P_{BS}$. Therefore, (35) becomes

$$\begin{aligned}\mathcal{P}_{D_2} &= \Pr\left\{\mathcal{H}_2{}^2 a_2 P_{BS} < \gamma_{th}\sigma^2\right\}\\ &= F_{\mathcal{H}_2^2}\left(\frac{\sigma^2\gamma_{th}}{a_2 P_{BS}}\right) = F_{\mathcal{H}_2}\left(\sqrt{\frac{\sigma^2\gamma_{th}}{a_2 P_{BS}}}\right).\end{aligned} \quad (37)$$

Based on (33), we derive the first line of (17) from (37).

If $a_1 - \gamma_{th}a_2 < a_2$ or $\gamma_{th} > a_1/a_2 - 1$, we have $\min\{\mathcal{H}_2{}^2 P_{BS}(a_1-\gamma_{th}a_2), \mathcal{H}_2{}^2 a_2 P_{BS}\} = \mathcal{H}_2{}^2 P_{BS}(a_1-\gamma_{th}a_2)$. Therefore, (35) becomes

$$\begin{aligned}\mathcal{P}_{D_2} &= \Pr\left\{\mathcal{H}_2{}^2 P_{BS}(a_1-a_2\gamma_{th}) < \sigma^2\gamma_{th}\right\}\\ &= F_{\mathcal{H}_2^2}\left(\frac{\sigma^2\gamma_{th}}{P_{BS}(a_1-a_2\gamma_{th})}\right)\\ &= F_{\mathcal{H}_2}\left(\sqrt{\frac{\sigma^2\gamma_{th}}{P_{BS}(a_1-a_2\gamma_{th})}}\right).\end{aligned} \quad (38)$$

Based on (33), we derive the second line of (17) from (38). Combination of three above cases, e.g., $\gamma_{th} \le a_1/a_2 - 1$, $a_1/a_2 - 1 < \gamma_{th} < a_1/a_2$, and $\gamma_{th} \ge a_1/a_2$, we obtain (17). The proof is thus complete.

B. ASYMPTOTIC ANALYSIS

To obtain insights from the derived expressions, we provide the asymptotic expressions of the OPs at D_1 and D_2 of the IRS-mmWave-NOMA system. Specifically, by using $\Gamma(a,x) = \Gamma(a)\exp(-x)\sum_{n=0}^{a-1}\frac{x^n}{n!}$ [44], the OPs at D_1 and D_2 given in (16) and (17) can be, respectively, expressed as (39) and (40), as shown at the bottom of the next page. From [46, Eq. (20)], (39) and (40) can be, respectively, approximated as (41) and (42), as shown at the bottom of the next page. Then, we can derive the asymptotic expressions of OPs from (41) and (42) as (43) and (44), as shown at the bottom of the next page, respectively. From (43) and (44), we can easily derive the diversity order of the IRS-mmWave-NOMA system. Particularly, the diversity orders at D_1 and D_2 (denoted by $\mathcal{D}_{O1}$ and $\mathcal{D}_{O2}$, respectively) are, respectively, computed as $\mathcal{D}_{O1} = -\lim_{P_{BS}\to\infty}[\log(\mathcal{P}_{D_1})/\log(P_{BS})]$ and $\mathcal{D}_{O2} = -\lim_{P_{BS}\to\infty}[\log(\mathcal{P}_{D_2})/\log(P_{BS})]$. Based on (43) and (44), we obtain the $\mathcal{D}_{O1}$ and $\mathcal{D}_{O2}$ as $\mathcal{D}_{O1} = \frac{[\Theta_{\mathcal{H}_1}(1)]^2}{2\left(\Theta_{\mathcal{H}_1}(2)-[\Theta_{\mathcal{H}_1}(1)]^2\right)}$ and $\mathcal{D}_{O2} = \frac{[\Theta_{\mathcal{H}_2}(1)]^2}{2\left(\Theta_{\mathcal{H}_2}(2)-[\Theta_{\mathcal{H}_2}(1)]^2\right)}$.

IV. NUMERICAL RESULTS AND DISCUSSIONS

In this section, the OPs at far and near users of the IRS-mmWave-NOMA system are determined via derived expressions. Monte-Carlo simulations are provided to validate analytical theory by using MATLAB software and 10^7 channel realizations. Moreover, we also provide the OPs at D_1 and D_2 in the case without IRS, e.g., only BS-D_1/D_2 direct links. Unless stated otherwise, the parameters used to obtain the numerical results are set as $\gamma_{th} = 1$, $m_{|h_l|} = m_{|g_{li}|} = m_{|h_{BSD_i}|} = m = 3$, and $G_{tx} = G_{rx} = 5$ dB. The positions of BS, I, D_1, and D_2 are expressed via coordinations (x, y), where the positions of BS and I are fixed, e.g., $(x_{BS}, y_{BS}) = (0, 0)$ and $(x_I, y_I) = (40, 20)$. The noise power is expressed as [16], [40] $\sigma^2 = 10\log(B_W)+N_F+N_0$, where B_W, N_F, and N_0 are, respectively, the bandwidth, noise figure, and thermal noise power density. Similar to [16], [40], [43], we set $B_W = 1$ MHz, $N_F = 10$ dBm, and $N_0 = -174$ dBm/Hz. Other parameters are varied to determine their effects on the OPs at D_1 and D_2.

Fig. 2 illustrates the OPs at D_1 and D_2 versus P_{BS} (in dBm, dB in the following) for $a_1 = 0.6, a_2 = 0.4$, $L = 100$, $(x_{D_1}, y_{D_1}) = (70, 0)$, $(x_{D_2}, y_{D_2}) = (50, 0)$, and $f_c = 30$ GHz. In other words, the distances from BS to far and near users are, respectively, 70 and 50 m. The analytical curves (denoted by "Ana") of the OPs at D_1 and D_2 with IRS are obtained by using (16) and (17), respectively. In addition, the asymptotic curves (denoted by "Asy") are obtained by using (43) and (44), respectively. It is obvious from Fig. 2 that utilizing IRS greatly reduces the OPs of the IRS-mmWave-NOMA system. Specifically, at $P_{BS} = 15$ dB, the OPs at D_2 with and without IRS are 10^{-3} and 4×10^{-2}, respectively. In other words, the OP at D_2 with IRS is 40 times lower than that without IRS when $P_{BS} = 15$ dB. Similar to D_2, at $P_{BS} = 20$ dB, the OPs at D_1 with and without IRS are 1.6×10^{-3} and 3×10^{-2}, respectively. Additionally, if the OP target at D_1 and D_2 is 10^{-4}, BS only uses 17 and 22.5 dB with IRS while it has to use 24 and 28 dB without IRS. Therefore, the utilizing IRS greatly reduces the power consumption of the transmitter. On the other hand, with the investigated parameters, the OPs at D_2 is significantly lower than that at D_1. Thus, we should reallocate a_1 and a_2 to obtain the same performance of both users. Furthermore, the diversity orders at D_1 and D_2 observed from Fig. 2 coincide with the analysis in previous subsection.

Fig. 3 determines the effects of L on the OPs at D_1 and D_2 for three cases, e.g., $L = 100$, 150, and 200 reflecting elements. In Fig. 3, the power allocation coefficients are reallocated, e.g., $a_1 = 0.8$ and $a_2 = 0.2$. With these a_1 and a_2, the OPs at D_1 and D_2 are nearly similar, especially in the case without IRS. When L increases, the OP performance at D_1 and D_2 significantly improves. More specifically, at $P_{BS} = 10$ dB, the OPs at D_1 and D_2 reduces from 1.7×10^{-1} and 1.5×10^{-1} to 3.4×10^{-2} and 1.5×10^{-2}, respectively, when L increases from 100 to 150. When

$$\mathcal{P}_{D_1} \approx \begin{cases} 1-\exp\left(-\frac{\Theta_{\mathcal{H}_1}(1)}{\Theta_{\mathcal{H}_1}(2)-[\Theta_{\mathcal{H}_1}(1)]^2}\sqrt{\frac{\gamma_{th}\sigma^2}{P_{BS}(a_1-\gamma_{th}a_2)}}\right)\sum_{n=0}^{\frac{[\Theta_{\mathcal{H}_1}(1)]^2}{\Theta_{\mathcal{H}_1}(2)-[\Theta_{\mathcal{H}_1}(1)]^2}-1}\frac{1}{n!}\left(\frac{\Theta_{\mathcal{H}_1}(1)}{\Theta_{\mathcal{H}_1}(2)-[\Theta_{\mathcal{H}_1}(1)]^2}\sqrt{\frac{\gamma_{th}\sigma^2}{P_{BS}(a_1-\gamma_{th}a_2)}}\right)^n, & \gamma_{th} < \frac{a_1}{a_2}, \\ 1, & \gamma_{th} \geq \frac{a_1}{a_2}, \end{cases} \tag{39}$$

$$\mathcal{P}_{D_2} \approx \begin{cases} 1-\exp\left(-\frac{\Theta_{\mathcal{H}_2}(1)}{\Theta_{\mathcal{H}_2}(2)-[\Theta_{\mathcal{H}_2}(1)]^2}\sqrt{\frac{\gamma_{th}\sigma^2}{P_{BS}a_2}}\right)\sum_{n=0}^{\frac{[\Theta_{\mathcal{H}_2}(1)]^2}{\Theta_{\mathcal{H}_2}(2)-[\Theta_{\mathcal{H}_2}(1)]^2}-1} \\ \frac{1}{n!}\left(\frac{\Theta_{\mathcal{H}_2}(1)}{\Theta_{\mathcal{H}_2}(2)-[\Theta_{\mathcal{H}_2}(1)]^2}\sqrt{\frac{\gamma_{th}\sigma^2}{P_{BS}a_2}}\right)^n, & \gamma_{th} \leq \frac{a_1}{a_2}-1, \\ 1-\exp\left(-\frac{\Theta_{\mathcal{H}_2}(1)}{\Theta_{\mathcal{H}_2}(2)-[\Theta_{\mathcal{H}_2}(1)]^2}\sqrt{\frac{\gamma_{th}\sigma^2}{P_{BS}(a_1-\gamma_{th}a_2)}}\right)\sum_{n=0}^{\frac{[\Theta_{\mathcal{H}_2}(1)]^2}{\Theta_{\mathcal{H}_2}(2)-[\Theta_{\mathcal{H}_2}(1)]^2}-1} \\ \frac{1}{n!}\left(\frac{\Theta_{\mathcal{H}_2}(1)}{\Theta_{\mathcal{H}_2}(2)-[\Theta_{\mathcal{H}_2}(1)]^2}\sqrt{\frac{\gamma_{th}\sigma^2}{P_{BS}(a_1-\gamma_{th}a_2)}}\right)^n, & \frac{a_1}{a_2}-1 < \gamma_{th} < \frac{a_1}{a_2}, \\ 1, & \gamma_{th} \geq \frac{a_1}{a_2}, \end{cases} \tag{40}$$

$$\mathcal{P}_{D_1} \approx \begin{cases} 1-\left[1-\frac{1}{\left(\frac{[\Theta_{\mathcal{H}_1}(1)]^2}{\Theta_{\mathcal{H}_1}(2)-[\Theta_{\mathcal{H}_1}(1)]^2}\right)!}\left(\frac{\Theta_{\mathcal{H}_1}(1)}{\Theta_{\mathcal{H}_1}(2)-[\Theta_{\mathcal{H}_1}(1)]^2}\sqrt{\frac{\gamma_{th}\sigma^2}{P_{BS}(a_1-\gamma_{th}a_2)}}\right)^{\frac{[\Theta_{\mathcal{H}_1}(1)]^2}{\Theta_{\mathcal{H}_1}(2)-[\Theta_{\mathcal{H}_1}(1)]^2}}\right], & \gamma_{th} < \frac{a_1}{a_2}, \\ 1, & \gamma_{th} \geq \frac{a_1}{a_2}, \end{cases} \tag{41}$$

$$\mathcal{P}_{D_2} \approx \begin{cases} 1-\left[1-\frac{1}{\left(\frac{[\Theta_{\mathcal{H}_2}(1)]^2}{\Theta_{\mathcal{H}_2}(2)-[\Theta_{\mathcal{H}_2}(1)]^2}\right)!}\left(\frac{\Theta_{\mathcal{H}_2}(1)}{\Theta_{\mathcal{H}_2}(2)-[\Theta_{\mathcal{H}_2}(1)]^2}\sqrt{\frac{\gamma_{th}\sigma^2}{P_{BS}a_2}}\right)^{\frac{[\Theta_{\mathcal{H}_2}(1)]^2}{\Theta_{\mathcal{H}_2}(2)-[\Theta_{\mathcal{H}_2}(1)]^2}}\right], & \gamma_{th} \leq \frac{a_1}{a_2}-1, \\ 1-\left[1-\frac{1}{\left(\frac{[\Theta_{\mathcal{H}_2}(1)]^2}{\Theta_{\mathcal{H}_2}(2)-[\Theta_{\mathcal{H}_2}(1)]^2}\right)!}\left(\frac{\Theta_{\mathcal{H}_2}(1)}{\Theta_{\mathcal{H}_2}(2)-[\Theta_{\mathcal{H}_2}(1)]^2}\sqrt{\frac{\gamma_{th}\sigma^2}{P_{BS}(a_1-\gamma_{th}a_2)}}\right)^{\frac{[\Theta_{\mathcal{H}_2}(1)]^2}{\Theta_{\mathcal{H}_2}(2)-[\Theta_{\mathcal{H}_2}(1)]^2}}\right], & \frac{a_1}{a_2}-1 < \gamma_{th} < \frac{a_1}{a_2}, \\ 1, & \gamma_{th} \geq \frac{a_1}{a_2}, \end{cases} \tag{42}$$

$$\mathcal{P}_{D_1} \approx \begin{cases} \frac{1}{\left(\frac{[\Theta_{\mathcal{H}_1}(1)]^2}{\Theta_{\mathcal{H}_1}(2)-[\Theta_{\mathcal{H}_1}(1)]^2}\right)!}\left(\frac{\Theta_{\mathcal{H}_1}(1)}{\Theta_{\mathcal{H}_1}(2)-[\Theta_{\mathcal{H}_1}(1)]^2}\sqrt{\frac{\gamma_{th}\sigma^2}{a_1-\gamma_{th}a_2}}\right)^{\frac{[\Theta_{\mathcal{H}_1}(1)]^2}{\Theta_{\mathcal{H}_1}(2)-[\Theta_{\mathcal{H}_1}(1)]^2}} P_{BS}^{\frac{-[\Theta_{\mathcal{H}_1}(1)]^2}{2\left(\Theta_{\mathcal{H}_1}(2)-[\Theta_{\mathcal{H}_1}(1)]^2\right)}}, & \gamma_{th} < \frac{a_1}{a_2}, \\ 1, & \gamma_{th} \geq \frac{a_1}{a_2}, \end{cases} \tag{43}$$

$$\mathcal{P}_{D_2} \approx \begin{cases} \frac{1}{\left(\frac{[\Theta_{\mathcal{H}_2}(1)]^2}{\Theta_{\mathcal{H}_2}(2)-[\Theta_{\mathcal{H}_2}(1)]^2}\right)!}\left(\frac{\Theta_{\mathcal{H}_2}(1)}{\Theta_{\mathcal{H}_2}(2)-[\Theta_{\mathcal{H}_2}(1)]^2}\sqrt{\frac{\gamma_{th}\sigma^2}{a_2}}\right)^{\frac{[\Theta_{\mathcal{H}_2}(1)]^2}{\Theta_{\mathcal{H}_2}(2)-[\Theta_{\mathcal{H}_2}(1)]^2}} P_{BS}^{\frac{-[\Theta_{\mathcal{H}_2}(1)]^2}{2\left(\Theta_{\mathcal{H}_2}(2)-[\Theta_{\mathcal{H}_2}(1)]^2\right)}}, & \gamma_{th} \leq \frac{a_1}{a_2}-1, \\ \frac{1}{\left(\frac{[\Theta_{\mathcal{H}_2}(1)]^2}{\Theta_{\mathcal{H}_2}(2)-[\Theta_{\mathcal{H}_2}(1)]^2}\right)!}\left(\frac{\Theta_{\mathcal{H}_2}(1)}{\Theta_{\mathcal{H}_2}(2)-[\Theta_{\mathcal{H}_2}(1)]^2}\sqrt{\frac{\gamma_{th}\sigma^2}{a_1-\gamma_{th}a_2}}\right)^{\frac{[\Theta_{\mathcal{H}_2}(1)]^2}{\Theta_{\mathcal{H}_2}(2)-[\Theta_{\mathcal{H}_2}(1)]^2}} P_{BS}^{\frac{-[\Theta_{\mathcal{H}_2}(1)]^2}{2\left(\Theta_{\mathcal{H}_2}(2)-[\Theta_{\mathcal{H}_2}(1)]^2\right)}}, & \frac{a_1}{a_2}-1 < \gamma_{th} < \frac{a_1}{a_2}, \\ 1, & \gamma_{th} \geq \frac{a_1}{a_2}, \end{cases} \tag{44}$$

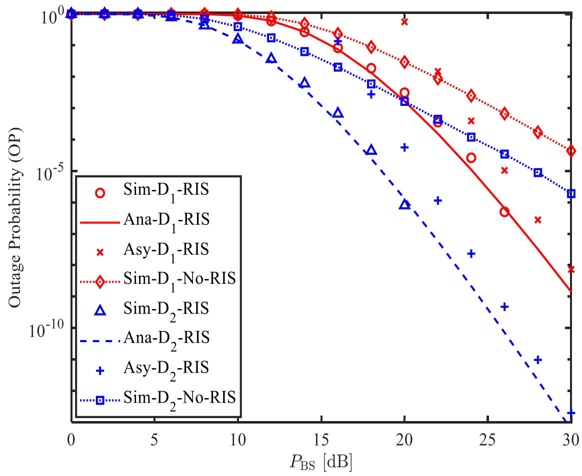

FIGURE 2. The OPs at D_1 and D_2 for $a_1 = 0.6$, $a_2 = 0.4$, $L = 100$, $(x_{D_1}, y_{D_1}) = (70, 0)$, $(x_{D_2}, y_{D_2}) = (50, 0)$, and $f_c = 30$ GHz.

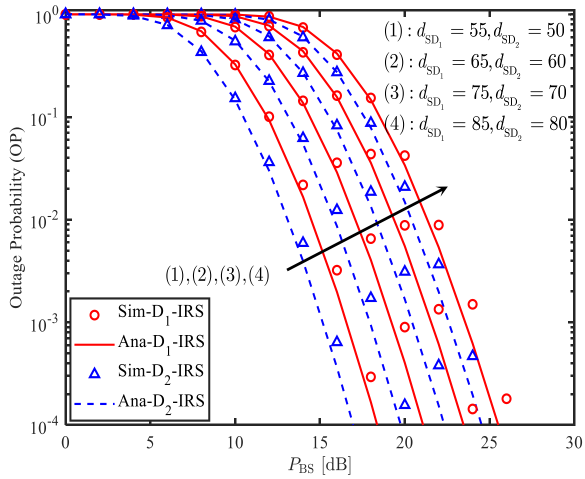

FIGURE 4. The OPs at D_1 and D_2 for $a_1 = 0.6$, $a_2 = 0.4$, $L = 100$, and $f_c = 30$ GHz.

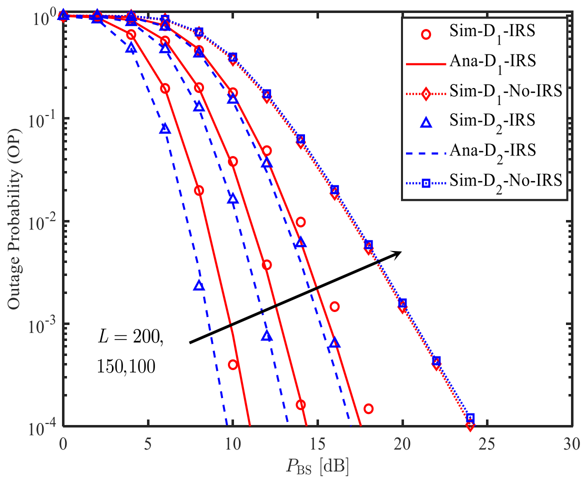

FIGURE 3. The effects of L on the OPs at D_1 and D_2 for $a_1 = 0.8$, $a_2 = 0.2$, $(x_{D_1}, y_{D_1}) = (70, 0)$, $(x_{D_2}, y_{D_2}) = (50, 0)$, and $f_c = 30$ GHz.

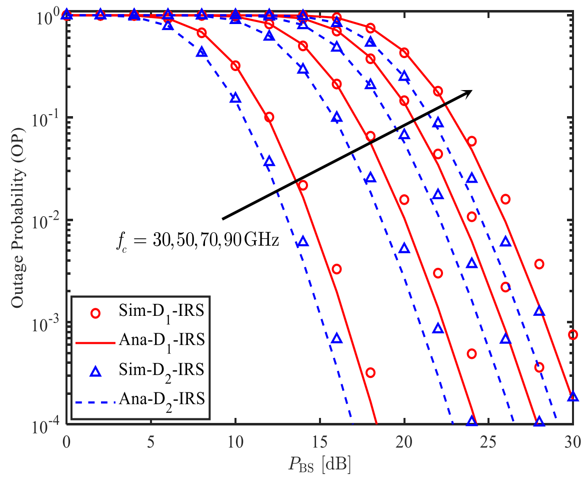

FIGURE 5. The impacts of f_c on the OPs at D_1 and D_2 for $a_1 = 0.6$, $a_2 = 0.4$, $L = 100$, $(x_{D_1}, y_{D_1}) = (55, 0)$, and $(x_{D_2}, y_{D_2}) = (50, 0)$.

$L = 200$, the OPs at D_1 and D_2 are, respectively, 8×10^{-3} and 10^{-4} at $P_{BS} = 10$ dB. An other observation is that when L increases, the differences between the OPs at D_1 and D_2 with IRS increase. Therefore, depending on L and the distances from BS to D_1 and D_2 in practice, we can choose appropriate values of a_1 and a_2 to obtain the required performance at two users. Notice that since Gamma approximations are used to obtain the OPs at D_1 and D_2 of the IRS-mmWave-NOMA system, the simulated and analytical results perfectly match in low transmit power regime. However, they are different in high transmit power regime. These results are reasonable and agreed with previous works [37], [39], [40].

In Fig. 4, the positions of D_1 and D_2 are varied in four cases, e.g., $(x_{D_1}, y_{D_1}) = (55, 0)$ and $(x_{D_2}, y_{D_2}) = (50, 0)$ (case 1), $(x_{D_1}, y_{D_1}) = (65, 0)$ and $(x_{D_2}, y_{D_2}) = (60, 0)$ (case 2), $(x_{D_1}, y_{D_1}) = (75, 0)$ and $(x_{D_2}, y_{D_2}) = (70, 0)$ (case 3), and $(x_{D_1}, y_{D_1}) = (85, 0)$ and $(x_{D_2}, y_{D_2}) = (80, 0)$ (case 4). In other words, the distances from BS to D_1 and D_2 are different in the four investigated cases. Since mmWave is used for the signal transmissions, increasing the BS-user distances significantly increases the OPs at D_1 and D_2. In particular, at $P_{BS} = 16$ dB, the OPs at D_1 and D_2 are 3×10^{-3} and 6×10^{-4}, 3.6×10^{-2} and 1.2×10^{-2}, 1.6×10^{-1} and 8×10^{-2}, and 4×10^{-1} and 2.7×10^{-1} corresponding to the cases 1, 2, 3, and 4. In other words, when the BS-user distances increases 10 m, the OPs nearly increase 10 times.

Fig. 5 evaluates the impacts of f_c on the OPs at D_1 and D_2 for $f_c = 30$, 50, 70, and 90 GHz. Similar to the distances, when f_c increases, the OPs at D_1 and D_2 greatly increase. In particular, at $f_c = 30$ GHz, the BS uses 18.2 and 17.6 dB to achieve OP $= 10^{-4}$ at D_1 and D_2, respectively. Meanwhile, for this OP target at D_1 and D_2, the BS has to use 24.1 and 23.2, 28 and 26.3, and 31 and 29 dB corresponding to $f_c = 50$, 70, and 90 GHz. In other words, when f_c increases from 30 to 50 GHz, the transmit power of BS has to increase 5.9 and 5.6 dB corresponding to users D_1 and D_2 dB to maintain OP $= 10^{-4}$. Moreover, the differences between

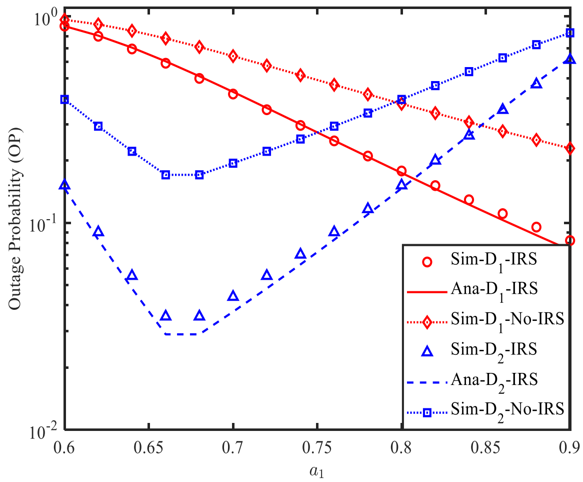

FIGURE 6. The OPs at D_1 and D_2 versus a_1 for $L = 100$, $f_c = 30$ GHz, $(x_{D_1}, y_{D_1}) = (70, 0)$, and $(x_{D_2}, y_{D_2}) = (50, 0)$.

OPs with $f_c = 30$ and 50 GHz are higher than those with $f_c = 50$ and 70 GHz, and $f_c = 70$ and 90 GHz.

Fig. 6 investigates the OPs at D_1 and D_2 versus a_1 for both with and without IRS. Notice that we have $a_2 = 1 - a_1$. We observe that with the considered parameters, the OPs at D_2 with and without IRS are minimum when $a_1 = 0.67$ and $a_2 = 0.33$. Meanwhile, the OPs at D_1 with and without IRS are minimum when $a_1 = 0.9$ and $a_2 = 0.1$. Moreover, the OPs at D_1 and D_2 with IRS are similar when $a_1 = 0.81$ and $a_2 = 0.19$. Meanwhile, in the case without IRS, the OPs at D_1 and D_2 are similar when $a_1 = 0.8$ and $a_2 = 0.2$. As the results, we can choose a suitable value of a_1 and a_2 to satisfy the OP requirements at D_1 and D_2 in practice.

V. CONCLUSION

In this paper, the performance of the IRS-mmWave-NOMA system was analyzed. We successfully derived the OP expressions at two users D_1 and D_2 under the impacts of practical conditions over Nakagami-m fading channels. Numerical results observed that the utilizing IRS significantly enhances the performance of the IRS-mmWave-NOMA system. In particular, for an OP target, the transmit power of BS with IRS is greatly lower than that without IRS. Moreover, for a specific transmit power, the OPs with IRS is considerably lower than those without IRS. Since the mmWave is used, increasing BS-user distances or carrier frequency leads to a significant decrease in the performance of the IRS-mmWave-NOMA system. Therefore, when the distances are far and the carrier frequency is extremely high, we can use an IRS with larger number of reflecting elements to maintain the performance of the IRS-mmWave-NOMA system. Moreover, we can reallocate the power coefficients of NOMA scheme to obtain the same performance at D_1 and D_2.

REFERENCES

[1] M. Ibrahim, S. Elhoushy, and W. Hamouda, "Uplink performance of mmWave-fronthaul cell-free massive MIMO systems," *IEEE Trans. Veh. Technol.*, vol. 71, no. 2, pp. 1536–1548, Feb. 2022.

[2] E. Iradier, A. Abuin, R. Cabrera, I. Bilbao, J. Montalban, P. Angueira, S. Kwon, N. Hur, and S.-I. Park, "Advanced NOMA-based RRM schemes for broadcasting in 5G mmWave frequency bands," *IEEE Trans. Broadcast.*, vol. 68, no. 1, pp. 143–155, Mar. 2022.

[3] L. Zhu, Z. Xiao, X.-G. Xia, and D. O. Wu, "Millimeter-wave communications with non-orthogonal multiple access for B5G/6G," *IEEE Access*, vol. 7, pp. 116123–116132, 2019.

[4] Y. Zhang, J. Mu, and J. Xiaojun, "Performance of multi-cell mmWave NOMA networks with base station cooperation," *IEEE Commun. Lett.*, vol. 25, no. 2, pp. 442–445, Feb. 2021.

[5] D. Zhang, Z. Zhou, C. Xu, Y. Zhang, J. Rodriguez, and T. Sato, "Capacity analysis of NOMA with mmWave massive MIMO systems," *IEEE J. Sel. Areas Commun.*, vol. 35, no. 7, pp. 1606–1618, Jul. 2017.

[6] Y. Xiu, J. Zhao, W. Sun, M. D. Renzo, G. Gui, Z. Zhang, and N. Wei, "Reconfigurable intelligent surfaces aided mmWave NOMA: Joint power allocation, phase shifts, and hybrid beamforming optimization," *IEEE Trans. Wireless Commun.*, vol. 20, no. 12, pp. 8393–8409, Dec. 2021.

[7] A. A. Amin and S. Y. Shin, "Capacity analysis of cooperative NOMA-OAM-MIMO based full-duplex relaying for 6G," *IEEE Wireless Commun. Lett.*, vol. 10, no. 7, pp. 1395–1399, Jul. 2021.

[8] Y. Cao, N. Zhao, G. Pan, Y. Chen, L. Fan, M. Jin, and M.-S. Alouini, "Secrecy analysis for cooperative NOMA networks with multi-antenna full-duplex relay," *IEEE Trans. Commun.*, vol. 67, no. 8, pp. 5574–5587, Apr. 2019.

[9] F. Guo, H. Lu, B. Li, D. Li, and C. W. Chen, "NOMA-assisted multi-MEC offloading for IoVT networks," *IEEE Wireless Commun.*, vol. 28, no. 4, pp. 26–33, Aug. 2021.

[10] T. Hou, Y. Liu, Z. Song, X. Sun, and Y. Chen, "MIMO-NOMA networks relying on reconfigurable intelligent surface: A signal cancellation-based design," *IEEE Trans. Commun.*, vol. 68, no. 11, pp. 6932–6944, Nov. 2020.

[11] F. Xu and H. Zhang, "Min-SINR maximization for mmWave massive MISO-NOMA system with randomly directional beamforming," *IEEE Access*, vol. 8, pp. 81997–82011, 2020.

[12] Y. Yapici, I. Guvenc, and H. Dai, "Low-resolution limited-feedback NOMA for mmWave communications," *IEEE Trans. Wireless Commun.*, vol. 19, no. 8, pp. 5433–5446, Aug. 2020.

[13] J. Ghosh, V. Sharma, H. Haci, S. Singh, and I.-H. Ra, "Performance investigation of NOMA versus OMA techniques for mmWave massive MIMO communications," *IEEE Access*, vol. 9, pp. 125300–125308, 2021.

[14] E. Basar, M. Di Renzo, J. De Rosny, M. Debbah, M. Alouini, and R. Zhang, "Wireless communications through reconfigurable intelligent surfaces," *IEEE Access*, vol. 7, pp. 116753–116773, 2019.

[15] M. A. El Mossallamy, H. Zhang, L. Song, K. G. Seddik, Z. Han, and G. Y. Li, "Reconfigurable intelligent surfaces for wireless communications: Principles, challenges, and opportunities," *IEEE Trans. Cogn. Commun. Netw.*, vol. 6, no. 3, pp. 990–1002, Sep. 2020.

[16] E. Björnson, O. Özdogan, and E. G. Larsson, "Intelligent reflecting surface versus decode-and-forward: How large surfaces are needed to beat relaying?" *IEEE Wireless Commun. Lett.*, vol. 9, no. 2, pp. 244–248, Feb. 2020.

[17] B. C. Nguyen, T. M. Hoang, L. T. Dung, and T. Kim, "On performance of two-way full-duplex communication system with reconfigurable intelligent surface," *IEEE Access*, vol. 9, pp. 81274–81285, 2021.

[18] B. C. Nguyen, T. M. Hoang, P. T. Tran, T. N. Nguyen, V.-D. Phan, B. V. Minh, and M. Voznak, "Cooperative communications for improving the performance of bidirectional full-duplex system with multiple reconfigurable intelligent surfaces," *IEEE Access*, vol. 9, pp. 134733–134742, 2021.

[19] V.-D. Phan, B. C. Nguyen, T. M. Hoang, T. N. Nguyen, P. T. Tran, B. V. Minh, and M. Voznak, "Performance of cooperative communication system with multiple reconfigurable intelligent surfaces over Nakagami-m fading channels," *IEEE Access*, vol. 10, pp. 9806–9816, 2022.

[20] Y. Zhuang, X. Li, H. Ji, and H. Zhang, "Exploiting intelligent reflecting surface for energy efficiency in ambient backscatter communication-enabled NOMA networks," *IEEE Trans. Green Commun. Netw.*, vol. 6, no. 1, pp. 163–174, Mar. 2022.

[21] A.-A. A. Boulogeorgos and A. Alexiou, "Performance analysis of reconfigurable intelligent surface-assisted wireless systems and comparison with relaying," *IEEE Access*, vol. 8, pp. 94463–94483, 2020.

[22] R. C. Ferreira, M. S. P. Facina, F. A. P. De Figueiredo, G. Fraidenraich, and E. R. De Lima, "Bit error probability for large intelligent surfaces under double-nakagami fading channels," *IEEE Open J. Commun. Soc.*, vol. 1, pp. 750–759, 2020.

[23] D. Selimis, K. P. Peppas, G. C. Alexandropoulos, and F. I. Lazarakis, "On the performance analysis of RIS-empowered communications over Nakagami-m fading," *IEEE Commun. Lett.*, vol. 25, no. 7, pp. 2191–2195, Jul. 2021.

[24] R. Zhong, Y. Liu, X. Mu, Y. Chen, and L. Song, "AI empowered RIS-assisted NOMA networks: Deep learning or reinforcement learning?" *IEEE J. Sel. Areas Commun.*, vol. 40, no. 1, pp. 182–196, Jan. 2022.

[25] H. Wang, C. Liu, Z. Shi, Y. Fu, and R. Song, "GSIC for RIS-aided uplink multi-antenna NOMA systems," *IEEE Commun. Lett.*, vol. 26, no. 1, pp. 187–191, Jan. 2022.

[26] Z. Tang, T. Hou, Y. Liu, J. Zhang, and C. Zhong, "A novel design of RIS for enhancing the physical layer security for RIS-aided NOMA networks," *IEEE Wireless Commun. Lett.*, vol. 10, no. 11, pp. 2398–2401, Nov. 2021.

[27] B. Tahir, S. Schwarz, and M. Rupp, "Analysis of uplink IRS-assisted NOMA under Nakagami-m fading via moments matching," *IEEE Wireless Commun. Lett.*, vol. 10, no. 3, pp. 624–628, Mar. 2021.

[28] X. Mu, Y. Liu, L. Guo, J. Lin, and H. V. Poor, "Intelligent reflecting surface enhanced multi-UAV NOMA networks," *IEEE J. Sel. Areas Commun.*, vol. 39, no. 10, pp. 3051–3066, Oct. 2021.

[29] Z. Li, M. Chen, Z. Yang, J. Zhao, Y. Wang, J. Shi, and C. Huang, "Energy efficient reconfigurable intelligent surface enabled mobile edge computing networks with NOMA," *IEEE Trans. Cognit. Commun. Netw.*, vol. 7, no. 2, pp. 427–440, Jun. 2021.

[30] X. Li, Z. Xie, Z. Chu, V. G. Menon, S. Mumtaz, and J. Zhang, "Exploiting benefits of IRS in wireless powered NOMA networks," *IEEE Trans. Green Commun. Netw.*, vol. 6, no. 1, pp. 175–186, Mar. 2022.

[31] M. Fu, Y. Zhou, Y. Shi, and K. B. Letaief, "Reconfigurable intelligent surface empowered downlink non-orthogonal multiple access," *IEEE Trans. Commun.*, vol. 69, no. 6, pp. 3802–3817, Jun. 2021.

[32] M. Elhattab, M.-A. Arfaoui, C. Assi, and A. Ghrayeb, "Reconfigurable intelligent surface assisted coordinated multipoint in downlink NOMA networks," *IEEE Commun. Lett.*, vol. 25, no. 2, pp. 632–636, Feb. 2021.

[33] A. S. de Sena, P. H. J. Nardelli, D. B. da Costa, F. R. M. Lima, L. Yang, P. Popovski, Z. Ding, and C. B. Papadias, "IRS-assisted massive MIMO-NOMA networks: Exploiting wave polarization," *IEEE Trans. Wireless Commun.*, vol. 20, no. 11, pp. 7166–7183, Nov. 2021.

[34] Y. Cheng, K. H. Li, Y. Liu, K. C. Teh, and H. Vincent Poor, "Downlink and uplink intelligent reflecting surface aided networks: NOMA and OMA," *IEEE Trans. Wireless Commun.*, vol. 20, no. 6, pp. 3988–4000, Jun. 2021.

[35] Q. Chen, M. Li, X. Yang, R. Alturki, M. D. Alshehri, and F. Khan, "Impact of residual hardware impairment on the IoT secrecy performance of RIS-assisted NOMA networks," *IEEE Access*, vol. 9, pp. 42583–42592, 2021.

[36] G. Alnwaimi and H. Boujemaa, "Non orthogonal multiple access using reconfigurable intelligent surfaces," *Wireless Pers. Commun.*, vol. 121, no. 3, pp. 1607–1625, Dec. 2021.

[37] F. Alanazi, "Non orthogonal multiple access with energy harvesting using reconfigurable intelligent surfaces for Rayleigh channels," *Wireless Pers. Commun.*, vol. 122, no. 3, pp. 2161–2181, Feb. 2022.

[38] A. Hemanth, K. Umamaheswari, A. C. Pogaku, D.-T. Do, and B. M. Lee, "Outage performance analysis of reconfigurable intelligent surfaces-aided NOMA under presence of hardware impairment," *IEEE Access*, vol. 8, pp. 212156–212165, 2020.

[39] S. Atapattu, R. Fan, P. Dharmawansa, G. Wang, J. Evans, and T. A. Tsiftsis, "Reconfigurable intelligent surface assisted two-way communications: Performance analysis and optimization," *IEEE Trans. Commun.*, vol. 68, no. 10, pp. 6552–6567, Oct. 2020.

[40] T. N. Do, G. Kaddoum, T. L. Nguyen, D. B. da Costa, and Z. J. Haas, "Multi-RIS-aided wireless systems: Statistical characterization and performance analysis," *IEEE Trans. Commun.*, vol. 69, no. 12, pp. 8641–8658, Dec. 2021.

[41] L. Yang, Y. Yang, D. B. D. Costa, and I. Trigui, "Outage probability and capacity scaling law of multiple RIS-aided networks," *IEEE Wireless Commun. Lett.*, vol. 10, no. 2, pp. 256–260, Feb. 2021.

[42] W. de Souza Junior and T. Abrao, "Outage performance of RIS-aided cooperative FD-SWIPT-NOMA in Nakagami-m channels," 2022, *arXiv:2204.01900*.

[43] I. Yildirim, A. Uyrus, and E. Basar, "Modeling and analysis of reconfigurable intelligent surfaces for indoor and outdoor applications in future wireless networks," *IEEE Trans. Commun.*, vol. 69, no. 2, pp. 1290–1301, Feb. 2021.

[44] A. Jeffrey and D. Zwillinger, *Table of Integrals, Series, and Products*. New York, NY, USA: Academic, 2007.

[45] D. L. Galappaththige, D. Kudathanthirige, and G. Amarasuriya, "Performance analysis of distributed intelligent reflective surface aided communications," in *Proc. IEEE Global Commun. Conf. (GLOBECOM)*, Taipei, Taiwan, Dec. 2020, pp. 1–6.

[46] Z. Wang and G. B. Giannakis, "A simple and general parameterization quantifying performance in fading channels," *IEEE Trans. Commun.*, vol. 51, no. 8, pp. 1389–1398, Aug. 2003.

NGUYEN VAN VINH was born in Binh Dinh, Vietnam, in 1984. He received the B.E. degree in computer science from Nha Trang University, Vietnam, in 2008, and the master's degree in computer science from the University of Transport and Communications, Vietnam, in 2015. He is currently a Lecturer with the Department of Information Assurance (IA), FPT University, Ho Chi Minh City, Vietnam. His research interests include wireless communication in 5G, networking, cybersecurity, physical layer security, and NOMA.

PHAN VAN TRI received the B.E. degree in mathematics and informatics from the University of Science, Vietnam National University Ho Chi Minh City, Vietnam, in 2005, the M.S. degree from Dalat University, Dalat, Vietnam, in 2010, and the Ph.D. degree from the University of Science, Vietnam National Ho Chi Minh City, in 2018. He is currently a Lecturer with the Ho Chi Minh Academy of Cryptography Techniques, Academy of Cryptography Techniques, Vietnam. His research interests include analytics, optimization theory, optimal control, MIMO, and communication.